

**Insights into the Biophysical Forces Between Proteins  
Involved in Elastic Fiber Assembly**

Journal:	<i>Journal of Materials Chemistry B</i>
Manuscript ID	TB-ART-06-2020-001591.R1
Article Type:	Paper
Date Submitted by the Author:	21-Aug-2020
Complete List of Authors:	Moore, Sean; Cleveland State University, Chemical and Biomedical Engineering Grubb, Tyler; Cleveland State University, Chemical and Biomedical Engineering Kothapalli, Chandrasekhar; Cleveland State University, Chemical and Biomedical Engineering

## **Insights into the Biophysical Forces Between Proteins Involved in Elastic Fiber Assembly**

Sean O'Neill Moore, Tyler Jacob Grubb, Chandrasekhar R. Kothapalli\*

Department of Chemical and Biomedical Engineering, Cleveland State University, Cleveland, OH 44115,  
USA

**\*Corresponding Author:** Chandrasekhar R. Kothapalli, PhD, Department of Chemical and Biomedical Engineering, FH 460, Cleveland State University, 2121 Euclid Avenue, Cleveland, OH 44115, USA. Tel: 1-216-687-2562. Email: [c.kothapalli@csuohio.edu](mailto:c.kothapalli@csuohio.edu)

ORCID ID: 0000-0001-8450-0640 (C. Kothapalli)

**ABSTRACT**

Elastogenesis is a complex process beginning with transcription, translation, and extracellular release of precursor proteins leading to crosslinking, deposition, and assembly of ubiquitous elastic fibers. While the biochemical pathways by which elastic fibers are assembled is known, the biophysical forces mediating the interactions between the constituent proteins is unknown. Using atomic force microscopy, we quantified the adhesive forces among the elastic fiber components, primarily between tropoelastin, elastin binding protein (EBP), fibrillin-1, fibulin-5, and lysyl oxidase-like 2 (LOXL2). The adhesive forces between tropoelastin and other tissue-derived proteins such as insoluble elastin, laminin, and type I collagens were also assessed. Adhesive forces between tropoelastin and laminin were strong ( $1767 \pm 126$  pN;  $p < 10^{-5}$  vs. all others), followed by forces ( $\geq 200$  pN) between tropoelastin and human collagen, mature elastin, or tropoelastin. Adhesive forces between tropoelastin and rat collagen, EBP, fibrillin-1, fibulin-5, and LOXL2 coated on fibrillin-1, were in the range 100 – 200 pN. The forces between tropoelastin and LOXL2, LOXL2 and fibrillin-1, LOXL2 and fibulin-5, and fibrillin-1 and fibulin-5 were less than 100 pN. Introducing LOXL2 decreased the adhesive forces between the tropoelastin monomers by  $\sim 100$  pN. The retraction phase of force-deflection curves was fitted to the Worm-Like Chain model to calculate the rigidity and flexibility of these proteins as they unfolded. Results provided insights into how each constituent's stretching under deformation contributes to structural and mechanical characteristics of these fibers, and to elastic fiber assembly.

**Key Words:** elastic fiber assembly, tropoelastin, atomic force microscopy, adhesive force, worm-like chain model, persistence length, contour length

## INTRODUCTION

Elastin is a critical extracellular matrix (ECM) protein that provides resilience and elasticity to tissues and organs.<sup>1</sup> It significantly contributes to the blood vessel expansion, blood flow regulation, functioning of the lung alveoli, and extensibility in the skin dermis, besides other critical functions in cartilage, tendons and ligaments.<sup>2,3</sup> Elastic fibers are durable macromolecules composed of an outer microfibrillar mantle and an inner core of elastin that makes up ~ 90% of the fiber (**Figure 1**).<sup>4</sup> They can be linearly stretched to 150% of their original length before rupture and are entropically driven by elastin's ability to stretch and recoil to the original state due covalent cross-linkages.<sup>3</sup> Elastic fiber assembly, i.e., elastogenesis, begins mid-gestation, completes during postnatal development, and undergoes very slow turnover in adult tissues. Post-transcription of elastin gene, tropoelastin monomers (~60-75 kDa non-glycosylated protein) rich in VGAP are translated on the rough endoplasmic reticulum by cleavage of the N-terminal signal peptide.<sup>1</sup> Post-translation, the  $\beta$ -galactosidase elastin-binding protein (EBP) attaches to tropoelastin monomers forming a complex, and guides within the cell to the plasma membrane, thereby preventing self-coacervation and degradation of tropoelastin. Once the tropoelastin-EBP complex is secreted onto the cell surface, EBP unbinds from tropoelastin and is recycled through the intracellular endosomal compartments, while the tropoelastin monomers accumulate by coacervation.<sup>5</sup> Tropoelastin aggregates are oxidized by lysyl oxidase (LOX) enzymes which drive their crosslinking by oxidative deamination of lysine side chains to allysine. Roughly 80% of lysine residues on tropoelastin participate in crosslinking and are found within the domains rich in alanine or proline.<sup>6</sup> Such crosslinked tropoelastin aggregates growing on the cell surface detach into the ECM and deposit onto the pre-existing microfibril (fibrillins-1, 2) scaffolds, *via* involvement of fibulin family that bind to full-length tropoelastin to increase the efficiency of coacervation.<sup>7, 8</sup> Tropoelastin deposition and LOX-mediated cross-linking continues until it is entirely incorporated into microfibrillar scaffolds.

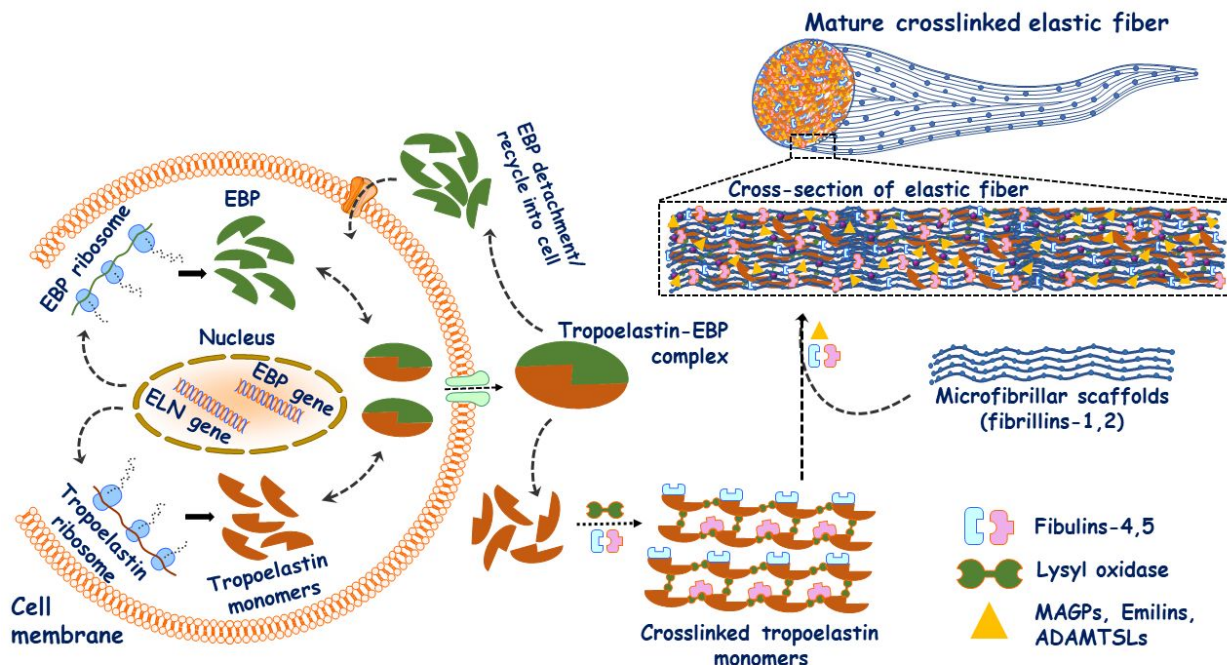


**Figure 1.** Schematic of the elastic fiber synthesis and deposition. Tropoelastin is translated *via* the ELN gene and is transported out of the cell by the elastin-binding protein (EBP). EBP detaches from tropoelastin once through the plasma membrane and recycled back into the cell, while tropoelastin coacervates and cross-links with help from fibulins-4, 5 and lysyl oxidase (LOX). Fibrillins make up the major structural microfibrillar component of the pre-existing scaffold, on which tropoelastin monomers deposit and crosslink further, until mature elastin is assembled to form elastic fibers. Numerous other components not depicted here also contribute to elastic fiber formation.<sup>9</sup> Note: Components not drawn to scale.

The microfibrillar scaffolds responsible for the elastic fiber assembly undergo N- and C- termini cleavage after secretion by tissue-specific cell types, and develop into the ~ 320 kDa mature forms.<sup>10</sup> The linear multimerization of fibrillins is achieved through the C-terminus domain at the cell surface and form bead-like structures, which further interact *via* N- and C- termini to form a parallel head-to-tail lateral structure.<sup>11, 12</sup> Finally, crosslinking of the fibrillin-rich microfibrils helps stabilize the scaffold on to which the lysine side chains of tropoelastin monomers bind.<sup>13</sup> Besides, elastic fibers also comprise and/or bind with microfibril-associated glycoproteins (MAGPs), fibronectin, latent TGF $\beta$ -binding proteins (LTBPs), nidogens – 1 and 2, and desmosine/ isodesmosine crosslinks, to name a few.<sup>8, 9, 14</sup>

Due to the inherent complexity associated with the organization of various proteins in elastic fiber assembly, coupled with attributes such as age, injury, or genetic mutations, many elastin-rich tissues are susceptible to malformation, degradation, and disease. For instance, incomplete microfibril scaffold

assembly leads to reduced tropoelastin cross-linking and elastic fiber formation<sup>15</sup>, point mutations of the elastin gene results in supraaortic stenosis<sup>16</sup>, deletion of exons in elastin gene results in Williams syndrome<sup>17</sup>, elastin gene transcript knockout results in blocked arteries<sup>3</sup>, elastic fiber loss and fragmentation leads to Marfan syndrome and Menkes disease<sup>18</sup>, fibrillin-1 mutations lead to abnormalities in cardiovascular, skeletal, and ocular systems<sup>19</sup>, fibrillin-2 mutations contributes to congenital contractual arachnodactyly<sup>9</sup>, atypical gathering of elastin fibers leads to pseudoxanthoma elasticum and Buschke-Ollendorff diseases<sup>3</sup>, and loss of elasticity and fiber degradation lead to diseases such as atherosclerosis and emphysema in the lungs and blood vessels<sup>20</sup>. Although the pathology (e.g., MMPs, elastases, inflammation, cytokines, chemokines) underlying degradation of mature elastic fibers is known, much remains to be uncovered, at both transcription and translational levels, on the alterations in protein structures and their biophysical interactions with other proteins leading to disorganized and random elastic fiber assembly in diseased tissues.

Prior studies employing a variety of characterization techniques (e.g., SFM, SAXS, SANS, AFM) offered insights into the structure-function relationship of elastic fiber associated proteins leading to diseases and disorders<sup>21-23</sup>. The affinity between tropoelastin and a few proteins in elastic fiber was investigated using solid-phase binding and surface plasmon resonance assays, which revealed that tropoelastin has a moderate affinity for fibulins<sup>24</sup>. MAGPs have been shown to have no binding with fibrillin-1 but bind to tropoelastin in the C-terminal region, while the N-terminal region of fibrillin-1 has a binding affinity to fibulin-2<sup>24</sup>. AFM has been established as an appropriate tool to study protein-protein and protein-ligand forces including specific and non-specific unbinding forces, off-rates, and binding energies<sup>25</sup>. For instance, the magnitude of unbinding forces between a variety of molecules is in the range of 15 – 1300 pN, when the pulling velocity of AFM tip is in 0.1 – 5  $\mu\text{m/s}$  range. Unbinding (adhesion) forces for proteins are low when only one protein interacts with a solid surface compared to when proteins interact with other protein-modified AFM tips. Using similar, established experimental approaches, we here report on the adhesive forces between some key proteins involved in elastogenesis.

Elastogenesis is a complex, organized, conserved, and regulated process, best defined as a sequence of protein-protein interactions. Elucidating the interactions underlying elastogenesis, especially at the molecular level, allows greater understanding of how deletions or mutations in critical proteins during disorders or diseases alter elastic tissue formation and functionality. Since the crystal structures of most of these proteins (*e.g.*, tropoelastin, fibrillin-2, fibulin-5, EBP) have not been elucidated yet, it is hard to implement computational tools (*e.g.*, molecular dynamic simulations) to qualitatively and quantitatively assess the molecular and structural interactions as well as the biophysical forces among the key proteins involved in elastogenesis. Thus, the objective of this study is to measure the adhesive forces that might be controlling the protein interactions between various critical components of the elastic fiber assembly, using an atomic force microscope (AFM). Such critical understanding of the forces between individual proteins in elastic fiber deposition process could help establish their contributions to matrix deposition and assembly, and cell-elastin interactions under healthy and diseased conditions. We discuss the implications of the results and possible mechanisms of elastic fiber formation, as well as propose improvements for future experimental and computational approaches. Although preliminary in scope, our observations bridge the gap between known biochemical processes and hitherto unknown biophysical forces contributing to elastic fiber assembly. These results have applications in bioengineering of elastomeric tissues, design of biomimetic scaffolds that stimulate elastin synthesis and elastic fiber regeneration in diseased or injured tissues, and customized gene therapies. Our approach could be extended to measure biophysical forces underlying other such macromolecular assemblies in physiological systems.

## EXPERIMENTAL SECTION

**Coating AFM cantilever tip.** Human recombinant tropoelastin containing one-third glycine amino acids and several lysine derivatives was purchased from Advanced Biomatrix (Carlsbad, CA, USA). Stock solution (1 mg/mL) was prepared by adding 0.25% glacial acetic acid to tropoelastin, further diluted in 0.25% acetic acid to 20  $\mu\text{g/mL}$  concentration, and stored at 5 °C. Recombinant human lysyl oxidase

homolog 2 protein (LOXL2; R&D Systems, Minneapolis, MN, USA) was diluted to 1  $\mu\text{g}/\text{mL}$  in 1 $\times$  PBS and stored at  $-80\text{ }^{\circ}\text{C}$ . Human fibulin-5, derived and cultured from the HEK-293 EBNA cell line, was a kind gift from Prof. Clair Baldock (The University of Manchester, UK). The as-received protein solution (40  $\mu\text{g}/\text{mL}$ ) was diluted to 20  $\mu\text{g}/\text{mL}$  in PBS, and stored at  $-80\text{ }^{\circ}\text{C}$ . A 5  $\mu\text{L}$  aliquot of tropoelastin, LOXL2, or fibulin-5 was coated on TR400PSA silicon nitride Cr/Au (5/30) AFM pyramidal cantilever tips (Olympus America Inc., Center Valley, PA, USA) and incubated at  $37\text{ }^{\circ}\text{C}$  for 3 h. The protein-coated cantilever tip was rinsed with PBS prior to AFM study. To verify protein deposition onto the AFM tip, immunofluorescence imaging of the tips was done using a Zeiss Axio Vert.A1 epi-fluorescence microscope. The protein-coated tips were washed with 1 $\times$  PBS, incubated with respective primary and secondary antibodies for each protein, and imaged after a final wash in 1 $\times$  PBS (**Figure S1**). The primary antibodies for human LOXL2, human tropoelastin, and human fibulin-5 were from Abcam (ab96233, ab21600, ab66339, respectively). Respective secondary antibodies were also from Abcam as appropriate.

**Coating cover glass substrates.** Recombinant human GLB-1 protein (0.5  $\text{mg}/\text{mL}$ ; Abcam, Cambridge, MA, USA), which has similar amino acid sequence as EBP, was diluted to 50  $\mu\text{g}/\text{mL}$  in 1 $\times$  PBS. Human fibulin-5/DANCE (20  $\mu\text{g}/\text{mL}$ ) and recombinant human fibrillin-1 protein (0.12  $\text{mg}/\text{mL}$ ; Abcam) diluted to 50  $\mu\text{g}/\text{mL}$  in 1 $\times$  PBS were used. Insoluble, mature, human aortic elastin (1  $\text{mg}$ ; Elastin Products Inc., Owensville, MO, USA) was reconstituted to 20  $\text{mg}/\text{mL}$  in PBS. Mouse laminin-1 (Thermo Fisher Scientific, Waltham, MA, USA) was diluted to 1  $\text{mg}/\text{mL}$ , rat-tail derived type I collagen (Corning Life Sciences, Corning, NY, USA) to 50  $\mu\text{g}/\text{mL}$ , and purified human tissues derived collagen-1 (Advanced Biomatrix) to 50  $\mu\text{g}/\text{mL}$  concentrations (all in PBS) and stored at  $5\text{ }^{\circ}\text{C}$ .

An 18-mm micro-cover glass (VWR International, Radnor, PA) was first washed with PBS and attached to a 50 mm  $\times$  9 mm polystyrene petri dish with a polyvinyl acetate homopolymer adhesive and left to dry. A 5  $\mu\text{L}$  aliquot of each diluted protein solution (tropoelastin, GLB-1, LOXL2, fibrillin-1, fibulin-5,

mature elastin, mouse laminin-1, rat and human type I collagens) was coated onto the cover glass, incubated at 37 °C for 3 h, rinsed and submerged in 4 mL of PBS prior to AFM experiments.

Human recombinant tropoelastin and LOXL2 were diluted in PBS to desired concentrations as detailed earlier. To test the interaction of tropoelastin in the presence of LOXL2, 5  $\mu\text{L}$  of tropoelastin was coated on a cover glass, incubated at 37 °C for 3 h, rinsed with PBS, and coated with 5  $\mu\text{L}$  of LOXL2 in the same region. The cover glass was incubated a second time at 37 °C for 2 h, rinsed with PBS, placed in a polystyrene petri dish, and submerged in 4 mL of PBS prior to testing with AFM. All experimental coating conditions for various protein coating configurations were listed in **Table S1**.

**FTIR spectroscopy analysis.** FTIR analysis of protein-coated cover glasses was performed using a Spectrum Two FT-IR Spectrometer (PerkinElmer Inc., Waltham, MA, USA) equipped with a Lithium Tantalate MIR detector to qualitatively detect protein deposition. Spectra were collected over the range of 8,300  $\text{cm}^{-1}$  to 350  $\text{cm}^{-1}$  with a spectral resolution of 0.5  $\text{cm}^{-1}$ . A single-beam background spectrum was collected from the cover glass with no protein coating, which served as the control. A single-beam sample spectrum for each subsequent protein coating was collected, with thorough cleansing of FTIR crystal using ethanol between the runs.

**Contact angle measurements.** To further confirm the presence of protein deposition on the cover glass, contact angle measurements based on sessile drop protocol were recorded using a Rame-Hart model 200 standard contact angle goniometer (Rame-Hart Instrument Co., Succasunna, NJ, USA). Briefly, 5  $\mu\text{L}$  of water was placed on the cover glass surface (pre-treated by manufacturer) containing each protein coating of interest<sup>26</sup>, and contact angle images taken within the first three seconds (to avoid hysteresis) with a super digital camera (Vivitar ViviCam 3750; 3.1 MP, 4 $\times$  digital zoom). Similar measurements were obtained from blank cover glass using demineralized water and ethanol droplets to establish static baseline contact angles for neutral and hydrophilic liquids. Multiple readings per protein coating were collected and the

image data was fit to the Young-Laplace equation using ImageJ's contact angle plug-in LBADSA. Representative contact angle images of various protein coated cover glasses were shown in **Figure S2**.

**Atomic force microscopy.** An atomic force microscope (MFP-3D BIO, Oxford Instruments, Santa Barbara, CA, USA) mounted on an inverted epi-fluorescence microscope (Nikon Eclipse Ti) was utilized to acquire force curves and adhesion data analysis. For protein-protein interaction studies, a TR400PSA silicon nitride Cr/Au (5/30) pyramidal cantilever tip (Olympus America Inc.) with a frequency  $\sim 34$  kHz, spring constant  $\sim 0.08$  N/m, and tip radius  $\sim 20$  nm was used. If the surface binding densities of the proteins were known, it would have helped in determining the appropriate protein concentration that would minimize multiple deposited proteins from simultaneously interacting with AFM tip. In lieu of that knowledge, we chose cantilevers with small tip radius to minimize the chance of multiple proteins interacting with the tip at any given time. For each experiment, spring constant was determined from a force-distance curve using thermal calibration method in a clean culture dish containing  $1\times$  PBS. Spring constant was determined both before and after the protein was coated on the cantilever, although coating did not affect spring constant values. For each experiment, a minimum of 50 utilizable force curves were obtained and the average adhesion force and standard error were calculated.

Force measurements were obtained using contact-mode on the protein-coated region of the cover glass (**Figure 3A**). The binding forces between non-coated AFM cantilevers and non-coated cover glass were compared to adhesion forces between protein-coated cover glass and blank AFM tip, and protein-coated cantilever tips and blank cover glass. These results set the baseline for the protein-protein interactions. AFM parameters (loading rate –  $10^5$  pN/s<sup>27</sup>; dwell time – 1 sec; trigger force – 1 nN) were chosen carefully to ensure that the tip does not interact simultaneously with multiple proteins, and were held constant for all experiments. Representative force-curves were shown in **Figure S3 (A)**. During retraction, the dissociation (i.e., unbinding or adhesion or rupture) force of the links was recorded till breakage of interaction bonds. Maximum adhesion force was measured as the difference between the maximum negative deflection and the position of zero cantilever deflection, using standard protocols from literature<sup>28, 29</sup>.

**Single protein characteristics.** The extensibility and stretch characteristics of proteins were computed using the Worm-like Chain (WLC) model, which relates the measured force to the extension of a protein through physical parameters such as persistence length and contour length<sup>30</sup>. Although this model has been widely used to fit single protein force spectroscopy measurements, we explored the utility of this model by fitting data obtained from our experimental setup, as our force-extension curves showed both single and multiple molecule stretching. Persistence length ( $L_P$ ) is defined as the distance in which two segments of a chain remain directionally correlated, i.e., protein chain's bending rigidity or local stiffness. Contour length ( $L_0$ ) is the fixed length of the chain, i.e., extension of the protein at rupture. The  $L_P$  and  $L_0$  of each protein were calculated from the WLC model using the equation:

$$F = \frac{k_B T}{L_P} \left[ \frac{1}{4 \left(1 - \frac{z}{L_0}\right)^2} - \frac{1}{4} + \frac{z}{L_0} \right]$$

where  $F$  is the adhesion force obtained from the force curve measurements,  $k_B$  is Boltzmann constant ( $1.38 \times 10^{-23}$  J.K<sup>-1</sup>),  $T$  is the temperature (K), and  $z$  is the extension of the protein before rupture. Regression analysis was ran using MATLAB (The MathWorks Inc., Natick, MA) to determine  $L_P$  and  $L_0$  using the initial guess of 0.5 nm and 150 nm, respectively. This model assumes that  $L_P \ll L_0$  and  $z > L_0$ . For  $L_P/L_0 \ll 1$ , the equation  $R_0 = \sqrt{2L_P L_0}$  gives the relationship between the mean squared end-to-end distance ( $R_0$ ) of a long, linear, polypeptide chain and the persistence and contour lengths assumed under the WLC assumptions<sup>31</sup>. As  $L_P \rightarrow \infty$ ,  $R_0^2 \approx L_0^2$ , the rigid rod limit, although not applicable for these proteins. Representative stretching curves for single or two molecules, fitted with the WLC model, is shown in **Figure S3-B**. Only after the initial portion of the curve (< 50 pN) was accurately fitted with the model,  $L_P$  which dictates the onset of the parabolic profile of the curve was obtained, although it may not visible in some cases as it is too close to the contact point. The empirical relationship between the hydrodynamic radius ( $R_h$  in Å) and the amino acid residues in native folded proteins is given by the equation  $R_h = 4.75 N^{0.29}$ , where  $N$  is the number of amino acid residues in the polypeptide chain<sup>32</sup> which was obtained from the respective manufacturers.

**Statistical analysis.** Data collected from contact angle, adhesion force, persistence length, and contour length were reported as mean  $\pm$  standard error for AFM data. Statistically significant differences ( $p$ -values) between cases were compared using Mann-Whitney-Wilcoxon test (for analysis of two groups) or Kruskal Wallis with Dunn's multiple comparison (for analysis of more than two groups), and performed using GraphPad Prism 5.0 (GraphPad Software, Inc., San Diego, CA).

## RESULTS AND DISCUSSION

### Proteins involved in elastic fiber formation are hydrophilic in nature

Contact angle measurements of water and ethanol drops on a non-coated borosilicate cover glass (**Table 1; Figure S2**) agree with literature.<sup>26, 33</sup> Results demonstrate that proteins have formed a coating layer on the glass surface and would interact with AFM tip upon close contact. All the protein-coated cover glasses exhibited hydrophilicity ( $20 < \theta < 90$ ) suggesting the exposure of hydrophilic side chain groups to the air-interface. The contact angles we measured for laminin-1 and type I collagen-coated cover glasses agree with literature,<sup>34, 35</sup> validating our contact angle measurements.

**Table 1.** Characteristics of the proteins and substrate surfaces. Contact angle measurements using a Rame-Hart model 200 standard contact angle goniometer for various proteins coated on borosilicate cover glass. The respective molecular weights and number of amino acid residues in the polypeptide sequence for proteins were listed.

Droplet content	Glass slide coating	MW, kDa	Number of residues <sup>a</sup>	Contact angle (°)
Ethanol	None			19.9 $\pm$ 1.4
distilled water	None			69.5 $\pm$ 1.4
distilled water	tropoelastin	68	618	80.0 $\pm$ 1.4
distilled water	GLB-1	74	672	63.5 $\pm$ 1.5
distilled water	fibulin-5	64	582	61.3 $\pm$ 1.9
distilled water	LOXL2	86	781	60.5 $\pm$ 2.2
distilled water	fibrillin-1	37	336	53.1 $\pm$ 2.1
distilled water	laminin-1	850	7727	27.4 $\pm$ 4.8
distilled water	rat collagen	139	1264	47.7 $\pm$ 1.2
distilled water	human collagen	129	1173	44.1 $\pm$ 1.1

<sup>a</sup>Unless specifically stated by the manufacturer, the number of amino acids in the protein chain was determined based on 0.11 kDa as the average molecular weight for each amino acid. Refer to Methods section for more details on each protein listed here.

Key proteins involved in elastic fiber formation (fibrillin-1, GLB-1, and fibulin-5) had relatively higher contact angles suggesting that they consist of some hydrophobic regions as well.<sup>36,37</sup> Fibrillin-1 is composed of repeat cysteine-rich chains which fold and stabilize by disulfide bonds.<sup>37</sup> This unique folding of a cysteine-rich hydrophobic core and short segments of proline and glycine help facilitate intramolecular and intermolecular interactions between fibrillin-1 and tropoelastin providing a structural scaffold for elastin synthesis.<sup>37,38</sup> A contact angle closer to that of water on plain cover glass suggests the hydrophobic regions of cysteine and proline dominate the structural composition while still allowing hydrophilic side chains to participate in hydrogen bonding. Our findings suggest a compact spread of fibrillin-1 on borosilicate glass, which explains the lower contact angle than proteins such as laminin and type I collagen.<sup>37</sup> GLB-1 binds to the VGVAPG domain of tropoelastin<sup>39</sup> and transports it out of the cell, preventing the mildly hydrophobic tropoelastin protein from untimed self-aggregation or degradation. Our results suggest that the side chains of GLB-1 associated with binding to tropoelastin might have repeating units. Fibulin-5 strongly interacts with proteins such as fibrillin-1, LOX, and tropoelastin *via* its repeating cbEGF motifs,<sup>40</sup> which might explain the close range of contact angles for all these proteins.

Similar to GLB-1 and fibrillin-1, the enzymatic role of LOXL2 is predicated on its binding and interaction with tropoelastin. Mature human LOX has the dominant hydrophobic regions buried in the protein core, leaving only a small fraction of hydrophilic side chains on the exposed surface.<sup>41</sup> Thus, the contact angle represents a slight hydrophilic characteristic. Tropoelastin consists of alternating hydrophilic and hydrophobic side chains which undergo hydrophobic interactions with LOX, fibrillin-1, and other tropoelastin monomers during coacervation.<sup>42</sup> The contact angle of tropoelastin could be representative of the chemical makeup of the dominating four hydrophobic amino acids (Gly, Val, Ala, Pro).

### **FTIR spectra measurements confirm the presence of protein coatings**

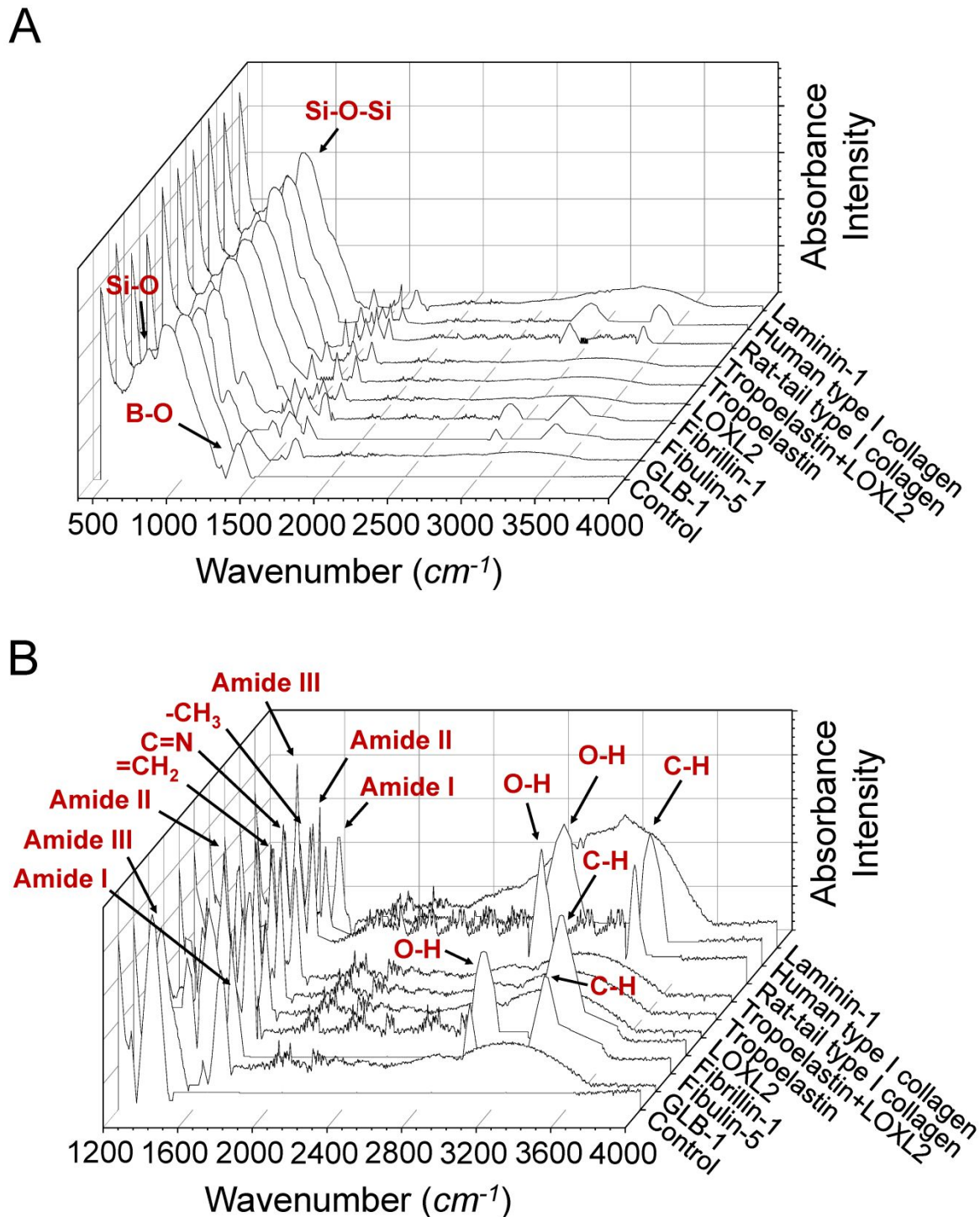


**Figure 2.** FTIR absorption intensities in (A) 500 – 4000  $cm^{-1}$  and (B) 1200 – 4000  $cm^{-1}$  range obtained using a Spectrum Two FT-IR Spectrometer. All samples show characteristic absorption peaks at  $\sim 1000$   $cm^{-1}$  and  $\sim 850$   $cm^{-1}$  which represent the silicon-oxygen-silicon stretching and silicon-oxygen peaks inherent of the non-coated borosilicate cover glass.

All samples showed characteristic FTIR absorption peaks at  $\sim 1400\text{ cm}^{-1}$ ,  $\sim 1000\text{ cm}^{-1}$ , and  $\sim 850\text{ cm}^{-1}$  representing B-O stretching, Si-O-Si stretching, and Si-O peaks, respectively (**Figure 2A**) inherent to the cover glass.<sup>43, 44</sup> Other key glass substrate absorption peaks were seen at wavelengths  $< 1000\text{ cm}^{-1}$ . The B-O peak also overlapped with amide III functional groups present in the proteins. The zoomed region of the spectra from  $1200 - 4000\text{ cm}^{-1}$  depicts the prominent peaks for each protein (**Figure 2B**). Fibrillin-1 specific peaks were noted at  $\sim 3333\text{ cm}^{-1}$  and  $\sim 2917\text{ cm}^{-1}$  (**Figure S4, A**) representing O-H groups and C-H bonds, respectively.<sup>45</sup> Many ECM proteins such as fibulin-5 exhibit similar functional groups. Peaks at  $\sim 1700\text{ cm}^{-1}$  represent amide I groups,  $\sim 1550\text{ cm}^{-1}$  represent amide II groups, while those  $\sim 1427\text{ cm}^{-1}$  and  $\sim 1375\text{ cm}^{-1}$  represent amide III group.<sup>45</sup> Similarly, since fibrillin-1 and GLB-1 both bind hydrophobically in nature to tropoelastin, FTIR analysis suggests that similar peaks would be seen in corresponding regions. Although GLB-1 shows intensity peaks at amide I and III regions, it does not have an amide II group as seen from the lack of intensity at  $\sim 1550\text{ cm}^{-1}$  (**Figure S4, A**).

Individual amide I, II, and III peaks were noted for LOXL2, tropoelastin, and when both these proteins were coated on top of each other (**Figure S4, B**). Tropoelastin has C=O bonds at  $1750 - 1650\text{ cm}^{-1}$  and a dominating peak at  $\sim 1530\text{ cm}^{-1}$ .<sup>46</sup> LOXL2 has dominating peaks at wavelengths of  $\sim 1346\text{ cm}^{-1}$  and  $\sim 1530\text{ cm}^{-1}$  suggesting the presence of lysine tyrosylquinone involved in the enzymatic activity needed to cross-link tropoelastin.<sup>47</sup> Overlapping intensities for both tropoelastin and LOXL2 seem to increase in intensity when both proteins were coated on the same cover glass, suggesting that as binding between these proteins occur, the functional groups of LOXL2 are not functionally altered, which is a characteristic of its enzymatic nature. Individual peaks associated with rat and human tissues derived type I collagen (**Figure S4, C**) suggest the presence of amide I, II, and III groups.<sup>48</sup> Laminin-1 also showed region-specific peaks at amide I, II, and III regions (**Figure S4, D**).<sup>49, 50</sup> Both rat and human collagen samples showed CH<sub>2</sub> and CH<sub>3</sub> bonds as well as C=N stretching bonds in the amide III region. These results, coupled with contact angle measurements, establish the presence of single and double layered protein coating on glass coverslips.

### Identification of strong, moderate, and weak adhesive forces between the proteins

The combinations of coated or non-coated AFM tip and cover slide tested in this study were depicted in **Figure 3A**. The frequency distributions of the data obtained in each case were shown in **Figures S5 – S10**. The adhesion force between clean, as-purchased, non-coated glass slide and a blank AFM tip was  $\sim 28.3 \pm 5.1$  pN (**Figure 3B, Figure S5**), while the tropoelastin-coated AFM tip recorded a significantly higher adhesion force  $\sim 51.4 \pm 6.4$  pN with an uncoated slide (**Figure 3C**;  $p = 0.0058$ ). These values serve as the baseline to compare force measurements observed in subsequent experiments under respective testing conditions. For the elastogenesis proteins (fibrillin-1, fibulin-5, tropoelastin, GLB-1, and LOXL2), the average adhesion force with the uncoated tip expectedly increased linearly with molecular weight ( $R^2 = 0.76$ ; **Figure 3B**). When tropoelastin and LOXL2 were sequentially coated on the same cover glass, the resulting complex had a higher molecular weight, and led to the highest adhesion forces amongst all tested cases with blank tip. Similarly, rat collagen, human collagen, and mouse laminin showed an increasing adhesion force with increasing molecular weight ( $R^2 = 0.84$ ; **Figure 3F**). The high-molecular weight proteins not associated with elastic fiber formation (collagens and laminin) had greater adhesion with the uncoated tip compared to the relatively lower molecular weight proteins involved in elastic fiber assembly.

In contrast to the forces noted with uncoated tip, the adhesion forces between proteins did not follow a linear increase with molecular weight when contacted with a tropoelastin-coated tip (**Figure 3C, Figure S6**). Adhesion force between tropoelastin-coated tip and tropoelastin-coated cover glass recorded the highest force ( $293.6 \pm 14.7$  pN), although tropoelastin has lower molecular weight than GLB-1 and LOXL2 and similar molecular weight to fibulin-5. While fibrillin-1 is roughly half the molecular size of GLB-1, both proteins showed similar adhesive forces with tropoelastin. Fibrillin-1 is cysteine rich which provides a hydrophilic environment for intermolecular interactions with tropoelastin. The intramolecular interaction within fibrillin-1 provides a scaffold on which tropoelastin could be deposited, and allows for relatively high adhesion with tropoelastin as it is further crosslinked.<sup>37, 38</sup> GLB-1, however, does not bind for long to tropoelastin and is merely a transport vesicle within the cell.<sup>39</sup> The adhesion forces between tropoelastin and GLB-1 seem to be dictated by the intermolecular forces between two molecules sharing similar size. Although LOXL2 is a cross-linker of tropoelastin molecules, the adhesion force between tropoelastin-

coated tip and LOXL2 coating on tropoelastin-covered glass (**Figure 3D**, **Figure S7**) was lower than the adhesion forces between two tropoelastin molecules in the absence of LOXL2 ( $p = 6.3E-5$ ; **Figure 3C**). Similarly, LOXL2 coating on fibrillin-1-coated cover glass showed non-significant (taking thermal noise into account) increase in the adhesive force with the tropoelastin-coated tip, compared to the interaction between tropoelastin and fibrillin-1 in the absence of LOXL2. Finally, (i) tropoelastin-coated tip interacting with uncoated cover slide has same adhesive forces as blank tip interacting with tropoelastin-coated slide, and (ii) mature elastin had higher adhesion with tropoelastin-coated tip than with blank tip.

Tropoelastin monomers will spontaneously aggregate on the cell surface once GLB-1 unbinds and is recycled back into the cell.<sup>5</sup> Tropoelastin strongly adhered to itself when coated on both the cover glass and AFM tip at a force double that with fibrillin-1 or GLB-1 (**Figure 3C**). The reason for such high adhesion force could be explained by the chemical bonds between allysine and lysine groups on tropoelastin molecules undergoing spontaneous crosslinking, either through condensation of two allysine residues *via* aldol condensation, or an allysine residue with a lysine residue *via* Schiff base reaction<sup>1</sup>. Subsequently, LOXL2 performs deamination cross-linking between allysine and lysine groups within tropoelastin. Our results show that introducing LOXL2 into the reaction decreased the adhesion forces between tropoelastin molecules (**Figure 3D**). Since ~80% of lysine residues on tropoelastin participate in the oxidation by LOX<sup>6</sup>, introducing LOXL2 on tropoelastin-coated cover glass probably led to the availability of only one-fifth of the lysine residues to interact with tropoelastin-coated AFM tip during the force measurements. Incubating tropoelastin-coated cover glass with LOXL2 must have led to spontaneous interactions and crosslinking of the lysine residues, resulting in lower adhesion forces, compared to LOXL2 absence where 100% of lysine residues are available for coacervation with other tropoelastin molecules.

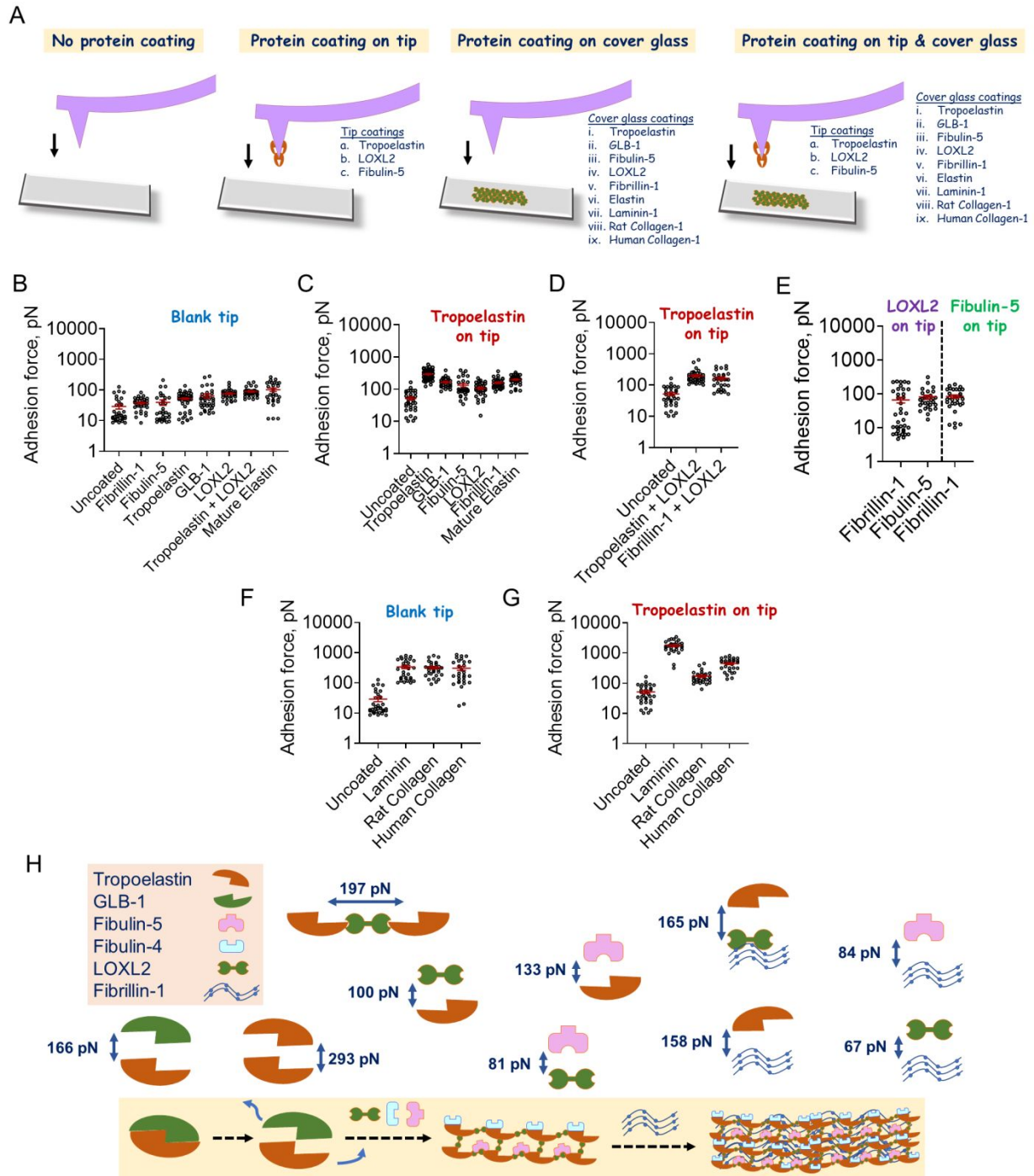


**Figure 3.** (A) Schematic of the experimental conditions implemented for AFM testing. Not listed are the conditions where more than one protein was coated on cover glass prior to AFM testing, although the method was similar to coating a single protein. Bee-swarm plots of the adhesion force measurements of proteins involved in elastic fiber synthesis using a (B) non-coated cantilever tip and (C) tropoelastin-coated tip. (D) Tropoelastin-coated tip was used to obtain adhesion force measurements when more than one protein was coated on the cover glass, primarily to assess the effect of cross-linker LOXL2. (E) Interaction of LOXL2 or fibulin-5 coated cantilever tip with fibrillin-1 and fibulin-5. (F) Non-coated cantilever tip or (G) tropoelastin-coated cantilever tip was used to measure adhesive forces of ECM proteins not involved

in elastic fiber synthesis, i.e., laminin and type I collagen. The open circle symbols represent the individual data points collected in each case, and the solid red lines represent the mean  $\pm$  SE. **(H)** Schematic summarizing the observed adhesive forces between various critical proteins (tropoelastin, fibrillin-1, fibulin-5, LOXL2, GLB-1) involved in elastic fiber assembly. The number of data points in respective cases were listed in **Table S2**.

The adhesive forces between LOXL2 and fibrillin-1 or fibulin-5 are less than the forces between tropoelastin and fibrillin-1 or tropoelastin and fibulin-5 (**Figure 3E, Figure S8**). The modestly higher adhesive forces between LOXL2 and fibulin-5 than that between LOXL2 and fibrillin-1 suggests a possible role for the combination of LOXL2 and fibulin-5 in accelerating tropoelastin coacervation. The adhesion force between tropoelastin and fibrillin-1 did not change in the presence of LOXL2 (**Figure 3D**) suggesting that the enzymatic activity of LOX is only limited to the aggregation and deposition of tropoelastin molecules<sup>1</sup>. Similarly, the average adhesion force between LOXL2 and fibrillin-1 (**Figure 3E**) was  $\sim 90$  pN lower than the interaction between tropoelastin and fibrillin-1. Others have shown no binding between immobilized LOX and N-terminal fibrillin-1.<sup>7</sup>

Tropoelastin binds to fibulin-5 through the N-terminal cbEGF domains and the C-terminal EB domains accelerating its coacervation.<sup>51</sup> The adhesion force between these two proteins was moderately less than that between tropoelastin and fibrillin-1. The higher average adhesion force between LOXL2 and fibulin-5 (vs. LOXL2 and fibrillin-1) might explain why fibulin-5 is a critical link between tropoelastin and fibrillin-1 and facilitate the correct deposition of LOX-tropoelastin complex onto a microfibrillar scaffold.<sup>51</sup> The adhesive forces between tropoelastin and ECM proteins (laminin and type I collagens) indicate that they have a higher adhesion force with tropoelastin compared to proteins involved in elastic fiber assembly (**Figure 3G, Figure S10**). Interestingly, tropoelastin-coated tip has (i) lower adhesion with mature elastin than with laminin or type I collagens, and (ii) higher adhesion with tropoelastin+LOXL2 substrate than blank tip interacting with tropoelastin+LOXL2 substrate.

No significant increases in adhesive forces were noted in all the cases tested at longer dwell times (3 or 5 sec). Higher dwell times could lead to alterations in the exposed surface areas of proteins as well as enhance the chances of multiple deposited proteins interacting simultaneously with AFM tip, while the drift

in the AFM tip has the potential to extend or decrease contact force with increasing dwell time.<sup>52</sup> Similar results were seen in experiments involving cell-protein adhesion forces.<sup>52</sup> Thus, determining the time-dependent protein interactions during the complex and prolonged process of elastic fiber deposition would be an arduous task. We maintained the tip loading rate constant ( $10^5$  pN/s) and the magnitude of forces we measured are comparable to literature.<sup>25, 53</sup> Our experiments established the specific interactions between tropoelastin and other proteins involved in elastic fiber formation and highlights the importance of specificity in binding necessary for assembly of healthy elastic matrix. **Figure 3H** depicts the average adhesion forces between the key proteins involved in elastogenesis based on our AFM results.

**Figure 4** summarizes all the known interactions between various prominent proteins (including, nidogens-1 and 2, MAGP-1, LTBP-2 and 4) involved in elastic fiber assembly identified by us and others, and obtained using various techniques (*e.g.*, solid phase binding, surface plasmon resonance, AFM).<sup>1, 24, 54-56</sup> Our AFM approach could be extended in the future to obtain the missing data (shown as boxes with cross marks) in the heat map. The trends in adhesive forces measured with AFM in our study is in tandem with binding forces reported by others using various assays, and could collectively lead to the following observations: (i) tight binding between GLB-1 and tropoelastin prevents coacervation, while strong binding forces between tropoelastin monomers maintains stability (Fig. 3C), (ii) fibrillin-1 interaction with tropoelastin dominates the elastin scaffold (Fig. 3C), while LOXL2 does not enhance fibrillin-tropoelastin binding (Fig. 3D), (iii) fibrillin-1 and tropoelastin primarily contribute to elastin stiffness, and (iv) LOXL2 has the ability to stretch before rupture, but seems to play little role in increasing protein forces and elastin stiffness (Fig. 3, D-E). Although adhesion forces could increase if very high concentrations of proteins were coated on the cover glass, we could not test it owing to protein insolubility at high concentrations, as well as unavailability in most cases. Besides, coating higher densities of proteins on the cover glass could promote simultaneous interactions between AFM tip and multiple deposited proteins, which is not desirable when quantifying the specific protein-protein interactions.

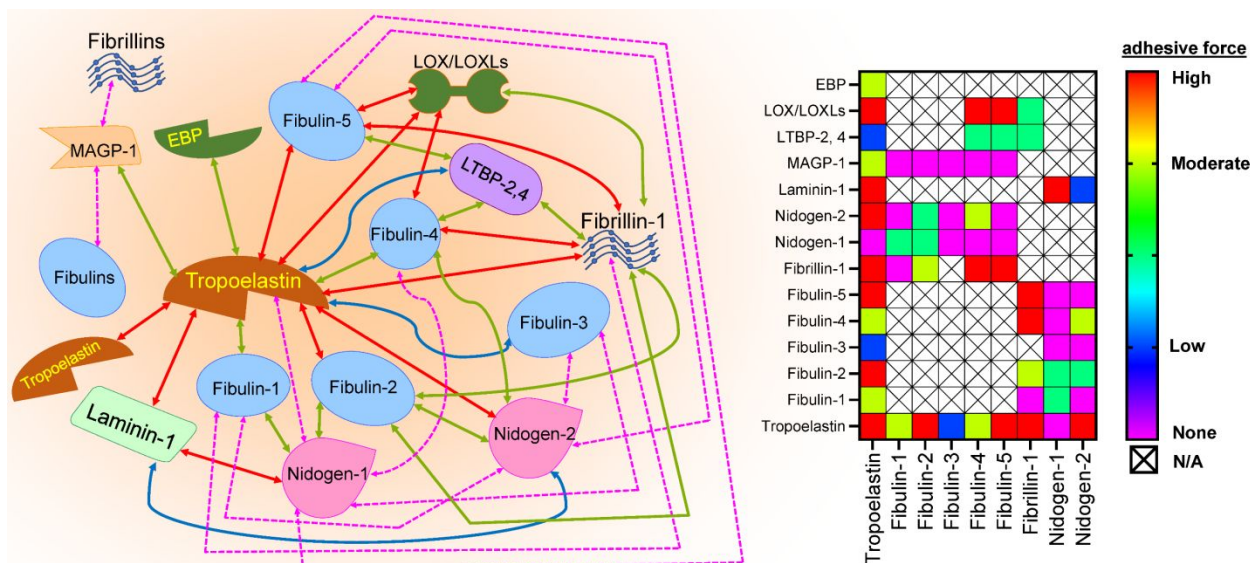


**Figure 4.** Schematic of the interactive forces between various proteins involved in elastic fiber formation, along with heat map of the strength of adhesive forces between those various proteins. Data was collated, compared, and plotted from our current study and those reported in literature using other characterization tools.<sup>24, 54-56</sup> The solid red lines represent strong interactions, solid green lines represent moderate forces, and solid blue lines represent weak interactions between the respective proteins, while the dashed pink lines represent no known interactions between the respective proteins. In the heat map, boxes with cross marks indicate lack of reported data on the interactions between those proteins.

### Characteristics of elastogenesis proteins computed from WLC model

Elastic fibers are continuously stretched and relaxed under physiological conditions and structurally flexible, yet they provide necessary rigidity and stiffness to tissues which undergo repetitive deformation. Force spectroscopy curves of elastic fiber proteins in our study were consistent with multiple molecule chains, however, none showed a sawtooth force pattern typical with the unfolding of titin Ig-like or spectrin  $\alpha$ -helical domains.<sup>57</sup> The best-fit measurements of WLC model were obtained for each force curve ( $R^2 > 0.95$ ) and the distributions of the lengths for each protein were shown in **Figure 5** ( $31 \leq n \leq 74$ ). While the force-extension curves from AFM analysis accurately depict the unfolding of individual protein domains, the *actual* contour lengths taking such domain unfolding into account can only be reached

experimentally at higher forces ( $> 100$  pN with AFM), and thus are typically estimated using elasticity models.<sup>58</sup>

Results suggest that our assumption of  $L_p \ll L_0$  is valid suggesting flexibility and extensibility in the chains of these polypeptides, and these chains do not reach full extension as  $L_p \ll R_0 < L_0$ . More than a single protein could rupture while the cantilever tip retracts and stretches the protein chains, as evident from multiple tethers noted in some force curves. Since the protein/complex structures are not known for most of these proteins, the  $L_p$  values we computed indicate the length of unstructured polypeptide chains appropriated in the binding interface. Similarly, the  $L_0$  we computed might account for only the amino acids which are force-bearing and not those hidden within the protein folds, common for these scenarios. It should be noted that extensible linker proteins (*e.g.*, PEG) were not used on the AFM tip or glass surface to tether the proteins in our study, although we plan to use that approach in our future studies. The range of  $L_p$  values for all the proteins ranged between 0.1 – 1 nm indicating that the neighboring amino acids are discernable. It should be noted that although side chains on proteins are not considered in the WLC model, they nevertheless could influence  $L_p$  values. Finally, the role of electrostatics and long-range interactions should not be overlooked, although their specific contributions could only be quantified by molecular dynamics stretching simulations under a variety of solvent conditions.

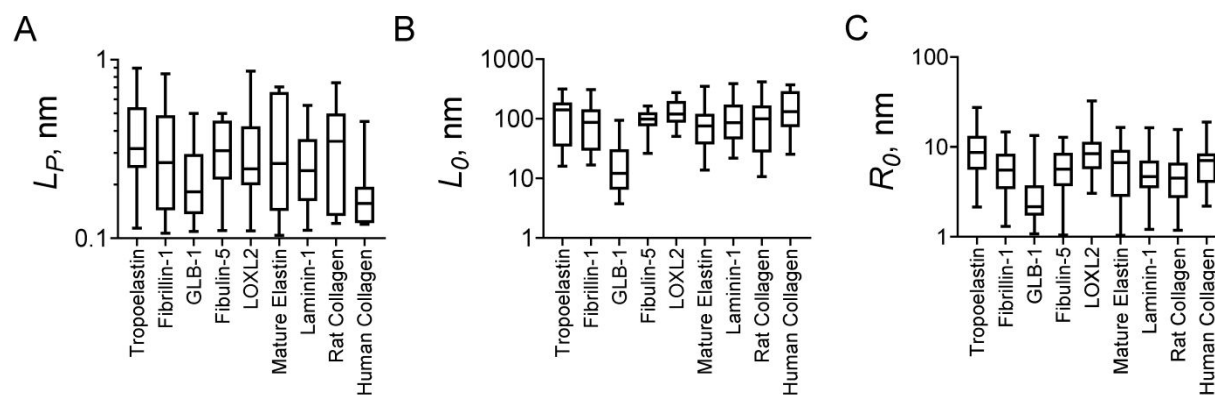


**Figure 5.** Box plots of the (A) persistence length ( $L_p$ ), (B) contour length ( $L_0$ ), and (C) squared end-to-end distance ( $R_0$ ) of protein chain measurements of various proteins fitted from the WLC model. The minimum, maximum, median, and range of these measurements for each protein are presented.

Our data suggests that (i) < 40% of force curves for fibrillin-1, GLB-1, LOXL2, and fibulin-5 showed multiple tethers, (ii) 50-60% of force curves showed multiple tethers for tropoelastin and mature elastin, and (iii) > 75% of the force curves for laminin and type I collagens showed multiple tethers. It is possible that laminin and collagens had a higher concentration on the cover glass as well as a higher molecular weight and therefore a greater chance for interaction with the tip leading to multiple tethers. The average  $L_0$  values indicate the inclusion of a few hundred amino acid residues in each case (length of an amino acid  $\approx 0.375$  nm). The average  $L_p$  and  $L_0$  values of tropoelastin we noted match those from repetitive AFM stretch and relaxation experiments.<sup>21</sup> The average  $L_p$  of tropoelastin was the highest among all elastogenesis proteins tested ( $p < 0.001$  vs. other proteins) while that of human collagens was the lowest ( $p < 0.001$  vs. all other proteins). Large  $L_p$  corresponds to protein chains with high stiffness, while low  $L_p$  suggests high flexibility. One explanation for the elasticity of tropoelastin lies in its chemical structure. Tropoelastin is a two-domain protein consisting of hydrophilic  $\alpha$ -helix heavy in Lys and Ala residues (the components driving LOX cross-linking) and hydrophobic  $\beta$ -turn regions heavy with VAGP residues.<sup>21</sup> The hydrophobic repeat domains of VPGVG and VGGVG are responsible for the elasticity and extensibility of tropoelastin.<sup>59</sup> The  $L_0$  of tropoelastin indicates the ability to stretch  $\sim 8\times$  than its folding length of  $\sim 20$  nm.<sup>21</sup> Tropoelastin is known to be a highly linear elastic protein and crosslinked tropoelastin hydrogels exhibit elasticity  $\sim 220$ - $280$  kPa.<sup>60</sup>

Fibrillin-1, known for its capacity to stretch, does not exhibit the same structural characteristics as tropoelastin, and is instead rich in cysteine and proline domains.<sup>42</sup> The intramolecular pleating model – explains the unfolding pattern of fibrillin-1 to rod-like regions that become undone as stretching occurs.<sup>61</sup> While a possible explanation, the fact that only 33% of fibrillin-1 force curves showed multiple chain breaks when undergoing stretch suggests involvement of another mechanism for fibrillin-1's unfolding pattern. The average  $L_0$  of laminin-1 was the highest ( $p < 0.05$  vs. all other proteins) while that of GLB-1 was the lowest ( $p < 0.001$  vs. other proteins, except fibulin-5). The  $L_0$  of various laminin types in solution was reported to be  $\sim 200$  nm,<sup>62</sup> while it was  $\sim 300$  nm for type I collagens,<sup>63</sup> which closely match our

observations. GLB-1 had the lowest  $L_P$  and  $L_0$  of all the tested proteins involved in elastic fiber synthesis, attesting to its non-specificity and insignificant role in the functionality of mature elastic fibers. An average  $L_0$  higher than fibrillin-1 and fibulin-5 suggests LOXL2 is capable of undergoing high deformation before rupture and is evidence that LOXL2 not only crosslinks tropoelastin but remains in the meshwork of elastic fiber assembly after cross-linking is achieved.<sup>1</sup> To our knowledge, this is the first attempt to compute the  $L_P$ ,  $L_0$ , and  $R_0$  of proteins widely involved in elastogenesis, and they are within range of other ECM proteins. Future studies should explore the changes in entropy and enthalpy values (i.e., thermodynamics) in these protein-protein interactions.

Even though the distributions of  $L_P$  values are very narrow (ranges within one order of magnitude) for all the proteins studied, the force spectroscopy measurements obtained here may not necessarily be from single molecules in each case, as the experiments were not specifically designed to that end. Rather, some of them could arise from lateral interactions between the proteins within each layer, so multiple protein interactions might be contributing to some of the adhesive force values. To overcome these limitations, our next phase of studies is geared towards tethering these proteins via flexible polymeric molecules using established protocols in literature, to obtain single molecule force spectroscopy measurements.

The hydrodynamic radius ( $R_h$ ) of a protein approximates the size of a 3D protein in its folded state and is a good representation of how large each protein is if it were globular before being stretched. Although it is typically measured using dynamic light scattering, it could be calculated based on the protein's molecular weight and the number of amino acid residues in the polypeptide chain to yield an approximation.<sup>32, 64</sup> ECM proteins not involved in elastic fiber formation had relatively larger  $R_h$  values compared to elastic fiber proteins due to higher residues in the sequence (**Table S3**). Mature elastin had a comparable  $R_h$  to tropoelastin likely due to folding of the mature elastin, while the highest  $R_h$  value was for laminin-1 due to its high molecular weight. These  $R_h$  values are within range reported for other proteins not involved in elastogenesis, as well as those derived from other experimental techniques.<sup>65</sup> Specifically, the  $R_h$  of tropoelastin is similar to that reported by Baldock *et al.*,<sup>21</sup> LOXL2 by Schmelzer *et al.*,<sup>66</sup> fibulin-5 by Jones *et al.*,<sup>67</sup> and fibrillin-1 by Baldock *et al.*,<sup>68</sup> after accounting for minor molecular weight differences.

## CONCLUSIONS

Elastogenesis is an integrated, sequential, and complex process of biophysical and biochemical interactions starting with extraction of proteins out of cells to their crosslinking and deposition, ultimately forming elastic fibers. This arduous process includes key interactions between many proteins including tropoelastin, MAGPs, EBP, fibulins, LOX, and fibrillins. AFM can reliably measure forces in the pN –  $\mu$ N range and thus could yield insights into the structural and energy landscapes of a variety of biomolecular complexes when deployed in pulling mode. Our studies revealed that the adhesion force among elastogenesis proteins increased with molecular weight for single protein extension studies. An uncoated AFM tip had strong interactions with cover slide coated with ECM proteins such as laminin and type I collagen. Interactions between tropoelastin monomers and other elastogenesis proteins depends on the specific role of each protein in elastic fiber assembly. Tropoelastin had stronger adhesive forces with other tropoelastin molecules as well as laminin-1 and type I collagen. Presence of LOXL2 did not enhance the adhesive forces between tropoelastin and fibrillin-1, suggesting the possible role of LOXL2 (and possibly other LOXs) only as the crosslinker of tropoelastin monomers. Fibrillin-5 interactions with tropoelastin, LOXL2, and fibrillin-1 suggests its overall role as a linker between tropoelastin and fibrillin-1, and further explains its role as a substrate-specific protein. Use of the WLC model gave insights into the contributions of tropoelastin and fibrillin-1 in elastic fiber's extensibility and flexibility under deformation.

Taken together, studies such as ours have significant applications in the bottom-up design of biomimetic elastomeric scaffolds for wound healing, tissue engineering, blood vessel replacement, and drug delivery, where the choice and characteristics of ingredients dictate the downstream mechanical and biological outcomes. Our study highlights the advantages of using theory and experiments synergistically to gain deeper understanding of single molecule biophysics as well as physiologically relevant hierarchical protein complexes. We believe that our current study barely scratched the surface of this topic, and after identification of the crystal structures of all the major proteins participating in elastic fiber assembly, molecular dynamics simulations could be implemented to guide and complement experiments that would lead to more clarity in our understanding of the complex biological processes such as elastogenesis.

## AUTHOR CONTRIBUTIONS

Chandra Kothapalli designed the study and provided all the resources. Sean Moore and Tyler Grubb performed the experiments. Sean Moore and Chandra Kothapalli wrote the manuscript with contributions from Tyler Grubb. All authors approved the final version of the manuscript.

## NOTES

The authors declare no competing financial interest.

## ACKNOWLEDGEMENTS

The authors acknowledge the support from the instrumentation core in the Chemistry department, and Dr. Nolan Holland's lab for sharing equipment at Cleveland State University. We thank Prof. Clair Baldock at the University of Manchester for generously sharing fibulin-5 protein, and Dr. Gautam Mahajan for his support with AFM training. This research was partially supported with funding from the faculty research development grant awarded to C.K. by the Office of Research at Cleveland State University, and the US National Science Foundation (CBET, Award # 1337859) to C.K.

## Supporting Information

The supporting information is available online

## REFERENCES

1. A. Ramamurthi and C. R. Kothapalli, *Elastic Fiber Matrices: Biomimetic Approaches to Regeneration and Repair*, CRC Press, Boca Raton, FL, First edn., 2016.
2. J. Rosenbloom, W. R. Abrams and R. Mecham, *FASEB J*, 1993, **7**, 1208–1218.
3. B. Vrhovski and A. S. Weiss, *Eur J Biochem*, 1998, **258**, 1-18.
4. R. P. Mecham and E. C. Davis, *Elastic fiber structure and assembly. In Extracellular Matrix Assembly and Structure*, Academic Press, New York, 1994.
5. R. P. Mecham, *Ann NY Acad Sci*, 1991, **624**, 137-146.
6. B. A. Kozel, H. Wachi, E. C. Davis and R. P. Mecham, *J Biol Chem*, 2003, **278**, 18491-18498.

7. R. Choudhury, A. McGovern, C. Ridley, S. A. Cain, A. Baldwin, M. C. Wang, C. Guo, A. Mironov, Z. Drymoussi, D. Trump, A. Shuttleworth, C. Baldock and C. M. Kielty, *J Biol Chem*, 2009, **284**, 24553-24567.
8. C. L. Papke and H. Yanagisawa, *Matrix Biol*, 2014, **0**, 142-149.
9. C. M. Kielty, M. J. Sherratt and C. A. Shuttleworth, *J Cell Sci*, 2002, **115**, 2817-2828.
10. D. M. Milewicz, J. Grossfield, S. N. Cao, C. Kielty, W. Covitz and T. Jewett, *J Clin Invest*, 1995, **95**, 2373-2378.
11. D. Hubmacher, E. I. El-Hallous, V. Nelea, M. T. Kaartinen, E. R. Lee and D. P. Reinhardt, *Proc Natl Acad Sci U S A*, 2008, **105**, 6548-6553.
12. A. Marson, M. J. Rock, S. A. Cain, L. J. Freeman, A. Morgan, K. Mellody, C. A. Shuttleworth, C. Baldock and C. M. Kielty, *J Biol Chem*, 2005, **280**, 5013-5021.
13. T. M. Trask, B. C. Trask, T. M. Ritty, W. R. Abrams, J. Rosenbloom and R. P. Mecham, *J Biol Chem*, 2000, **275**, 24400-24406.
14. J. Thomson, M. Singh, A. Eckersley, S. A. Cain, M. J. Sherratt and C. Baldock, *Semin Cell Dev Biol*, 2019, **89**, 109-117.
15. S. Kasamatsu, A. Hachiya, T. Fujimura, P. Sriwiriyanont, K. Haketa, M. O. Visscher, W. J. Kitzmiller, A. Bello, T. Kitahara, G. P. Kobinger and Y. Takema, *Sci Rep*, 2011, **1**, 164.
16. D. Y. Li, A. E. Toland, B. B. Boak, D. L. Atkinson, G. J. Ensing, C. A. Morris and M. T. Keating, *Hum Mol Genet*, 1997, **6**, 1021-1028.
17. M. C. Lowery, C. A. Morris, A. Ewart, L. J. Brothman, X. L. Zhu, C. O. Leonard, J. C. Carey, M. Keating and A. R. Brothman, *Am J Hum Genet*, 1995, **57**, 49-53.
18. J. Uitto and L. J. Ryhänen, *Pathology of the elastic fibers, in Connective tissue disease*, Dekker, New York, 1987.
19. C. Hayward and D. J. Brock, *Hum Mutat*, 1997, **10**, 415-423.
20. L. B. Sandberg, N. T. Soskel and J. G. Leslie, *N Engl J Med*, 1981, **304**, 566-579.
21. C. Baldock, A. F. Oberhauser, L. Ma, D. Lammie, V. Siegler, S. M. Mithieux, Y. Tu, J. Y. H. Chow, F. Suleman, M. Malfois, S. Rogers, L. Guo, T. C. Irving, T. J. Wess and A. S. Weiss, *Proc Natl Acad Sci U S A*, 2011, **108**, 4322-4327.
22. R. Flama, P. A. Zhdan, M. Martino, J. E. Castle and A. M. Tamburro, *Biomacromolecules*, 2004, **5**, 1511-1518.
23. I. Pasquali Ronchetti, A. Alessandrini, M. Baccarani Contri, C. Fornieri, G. Mori, D. Quagliano and U. Valdrè, *Matrix Biol*, 1998, **17**, 75-83.
24. T. Sasaki, W. Göhring, N. Miosge, W. R. Abrams, J. Rosenbloom and R. Timpl, *FEBS Lett*, 1999, **460**, 280-284.
25. C. K. Lee, Y. M. Wang, L. S. Huang and S. Lin, *Micron*, 2007, **38**, 446-461.
26. S. K. Reinke, K. Hauf, J. Vieira, S. Heinrich and S. Palzer, *J Phys D: Appl Phys*, 2015, **48**, 464001.
27. H. Tobimatsu, Y. Nishibuchi, S. Ryo, G. Shinya and T. Kazuo, *J Atheroscler Thromb*, 2015, **22**, 1091-1099.
28. H. J. Butt, B. Cappella and M. Kappl, *Surf Sci Rep*, 2005, **59**, 1-152.
29. E. L. Florin, V. T. Moy and H. E. Gaub, *Science*, 1994, **264**, 415-417.
30. C. Bouchiat, M. D. Wang, J. F. Allemand, T. Strick, S. M. Block and V. Croquette, *Biophys J*, 1999, **76**, 409-413.
31. J. F. Marko and E. D. Siggia, *Macromolecules*, 1995, **28**, 8759-8770.
32. D. K. Wilkins, S. B. Grimshaw, V. Receveur, C. M. Dobson, J. A. Jones and L. J. Smith, *Biochemistry*, 1999, **38**, 16424-16431.

33. C. Yu, C. Yu, L. Cui, Z. Song, X. Zhao, Y. Ma and L. Jiang, *Adv Mater Interfaces*, 2017, **4**, 1600862.
34. K. Miyake, K. Maekubo, S. Miyake, A. Yamauchi, H. Futamura, P. Gravagna and J. L. Tayot, *Eur J Imlant Refract Surg*, 1994, **6**, 132-137.
35. T. Wu, D. Li, Y. Wang, B. Sun, D. Li, Y. Morsi, H. El-Hamshary, S. S. Al-Deyab and X. Mo, *J Mater Chem B*, 2017, **5**, 3186-3194.
36. N. Brunetti-Pierri and F. Scaglia, *Mol Genet Metab*, 2008, **94**, 391-396.
37. F. Ramirez and L. Pereira, *Int J Biochem Cell B*, 1999, **31**, 255-259.
38. X. Yuan, A. K. Downing, V. Knott and P. A. Handford, *EMBO J*, 1997, **16**, 6659-6666.
39. A. Hinek and M. Rabinovitch, *J Cell Biol*, 1994, **126**, 563-574.
40. H. Yanagisawa, M. K. Schluterman and R. A. Brekken, *J Cell Commun Signal*, 2009, **3**, 337-347.
41. C. J. Krebs and S. A. Krawetz, *Biochim Biophys Acta*, 1993, **1202**, 7-12.
42. M. J. Rock, S. A. Cain, L. J. Freeman, A. Morgan, K. Melody, A. Marson, C. A. Shuttleworth, A. S. Weiss and C. M. Kielty, *J Biol Chem*, 2004, **279**, 23748-23758.
43. N. B. Colthup, L. H. Daly and S. E. Wiberley, *Introduction to Infrared and Raman Spectroscopy*, Academic Press, 1990.
44. K. T. Tan, C. C. White, D. L. Hunston, C. Clerici, K. L. Steffens, J. Goldman and B. D. Vogt, *J Adhesion*, 2008, **84**, 339-367.
45. K. O. Reddy, J. Zhang, J. Zhang and A. V. Rajulu, *Carbohydr Polym*, 2014, **114**, 537-545.
46. L. B. Dyksterhuis, E. A. Carter, S. M. Mithieux and A. S. Weiss, *Arch Biochem Biophys*, 2009, **487**, 79-84.
47. S. X. Wang, N. Nakamura, M. Mure, J. P. Klinman and J. Sanders-Loehr, *J Biol Chem*, 1997, **272**, 28841-28844.
48. C. Petibois, G. Gousspillou, K. Wehbe, J. P. Delage and G. Déléris, *Anal Bioanal Chem*, 2006, **386**, 1961-1966.
49. A. D. Meade, F. M. Lyng, P. Knief and H. J. Byrne, *Anal Bioanal Chem*, 2007, **387**, 1717-1728.
50. N. K. Zahari, R. B. H. Idrus and S. R. Chowdhury, *Int J Mol Sci*, 2017, **18**, E2242.
51. H. Yanagisawa and E. C. Davis, *Int J Biochem Cell Biol*, 2010, **42**, 1084-1093.
52. M. Benoit and H. E. Gaub, *Cells Tissues Organs*, 2002, **172**, 174-189.
53. Y. S. Lo, Y. J. Zhu and T. P. Beebe, *Langmuir*, 2002, **17**, 3741-3748.
54. N. Kobayashi, G. Kostka, J. H. Garbe, D. R. Keene, H. P. Bächinger, F. G. Hanisch, D. Markova, T. Tsuda, R. Timpl, M. L. Chu and T. Sasaki, *J Biol Chem*, 2007, **282**, 11805-11816.
55. R. Timpl, T. Sasaki, G. Kostka and M. L. Chu, *Nat Rev Mol Cell Biol*, 2003, **4**, 479-489.
56. Y. Yamauchi, E. Tsuruga, K. Nakashima, Y. Sawa and H. Ishikawa, *Acta Histochem Cytochem*, 2010, **43**, 131-138.
57. A. F. Oberhauser and M. Carrión-Vázquez, *J Biol Chem*, 2008, **283**, 6617-6621.
58. M. Carrion-Vazquez, P. E. Marszalek, A. F. Oberhauser and J. M. Fernandez, *Proc Natl Acad Sci U S A*, 1999, **96**, 11288-11292.
59. M. Guthold, W. Liu, E. A. Sparks, L. M. Jawerth, L. Peng, M. Falvo, R. Superfine, R. R. Hantgan and S. T. Lord, *Cell Biochem Biophys*, 2007, **49**, 165-181.
60. S. G. Wise, G. C. Yeo, M. A. Hiob, J. Rnjak-Kovacina, D. L. Kaplan, M. K. Ng and A. S. Weiss, *Acta Biomater*, 2014, **10**, 1532-1541.
61. Y. Lu, D. F. Holmes and C. Baldock, *J Mol Biol*, 2005, **349**, 73-85.

62. J. M. Szymanski, M. Ba and A. W. Feinberg, *J Mater Chem B*, 2015, **3**, 7993-8000.
63. Y. L. Sun, Z. P. Luo, A. Fertala and K. N. An, *Biochem Biophys Res Commun*, 2002, **295**, 382-386.
64. C. S. Tsai, *Biomacromolecules: Introduction to Structure, Function and Informatics*, Wiley, 2006.
65. M. Le Maire, A. Ghazi, J. V. Moller and L. P. Aggerbeck, *Biochem J*, 1987, **243**, 399-404.
66. C. E. H. Schmelzer, A. Heinz, H. Troilo, M. P. Lockhart-Cairns, T. A. Jowitt, M. F. Marchand, L. Bidault, M. Bignon, T. Hedtke, A. Barret, J. C. McConnell, M. J. Sherratt, S. Germain, D. J. S. Hulmes, C. Baldock and L. Muller, *FASEB J*, 2019, **33**, 5468-5481.
67. R. P. O. Jones, C. Ridley, T. A. Jowitt, M. C. Wang, M. Howard, N. Bobola, T. Wang, P. N. Bishop, C. M. Kielty, C. Baldock, A. J. Lotery and D. Trump, *Invest Ophthalmol Vis Sci.*, 2010, **51**, 2356–2362.
68. C. Baldock, V. Siegler, D. V. Bax, S. A. Cain, K. T. Mellody, A. Marson, J. L. Haston, R. Berry, M. C. Wang, J. G. Grossmann, M. Roessle, C. M. Kielty and T. J. Wess, *Proc Natl Acad Sci U S A*, 2006, **103**, 11922-11927.

The adhesive forces between various proteins involved in elastic fiber assembly was quantified using an atomic force microscope.

